VI International Conference on Particle-based Methods – Fundamentals and Applications
PARTICLES 2019
E. Oñate, M. Bischoff, D.R.J. Owen, P. Wriggers & T. Zohdi (Eds)

A METHODOLOGY OF A SENSITIVITY ANALYSIS IN DEM EXPERIMENTS

Momme Jahn[1] **and Martin Meywerk** [2]

[1]Helmut-Schmidt-University
Chair of Automotive Engineering
Holstenhofweg 85, 22043 Hamburg, Germany
e-mail: momme.jahn@hsu-hh.de

[2] Helmut-Schmidt-University
Chair of Automotive Engineering
Holstenhofweg 85, 22043 Hamburg, Germany
e-mail: martin.meywerk@hsu-hh.de

Key words: DEM, Sobol' Indices, Metamodels, Sensitivity Analysis, Particle Pile, Oedometer Test, Force-Controlled Plate, Angle Of Repose

Abstract. In this publication a sensitivity analysis for DEM modelparameters with respect to the pile- and the oedometer experiment is described. The analysis is performed with Sobol' indices. Since the huge computational effort of the corresponding DEM models different metamodels are used to determine these indices. The (RSM) metamodels are established by using Latin Hypercube sampling points.
A three-dimensional ansatz for the determination of the angle of repose as well as the algorithm of a force-controlled plate is described in order to get results for the pile- and the oedometer experiment.

1 INTRODUCTION

The Discrete-Element-Method (DEM) is a capable method to investigate huge deformations in granular media [23]. These could occur e.g. in tire-soil-interactions [7, 9], the flow of particles through hoppers [5].
A very important and challenging point is the identification of DEM-parameters. A common way for the parameter identification is the calibration of experiments. An often used experiment is the calibration of granular piles [2]. The angle of repose could be used to determine the accordance between the numerical pile and the experimental one. Another experiment is the oedometer test, which is a one-dimensional compression test where the horizontal displacement of the soil is prevented [16, 10]. This test is used to investigate the stress-displacement behavior [13, p. 252]. Often the calibration process is done with a trial-and-error procedure despite its disadvantages with the high number of parameters [11, p. 73]. A more appropriate calibration process could be performed if the influence of parameters and their interactions are known [2, p. 333] e.g. if some parameters have a negligible influence, they could be neglected in

the parameter calibration process. In order to determine the influence of parameters and their interactions a sensitivity analysis is performed with Sobol' indices [3, p. 1]. Sobol's indices are a common used for sensitivity measurements[17, p. 964].
The determination of the angle of repose is performed in [11, p. 74] with an image processing algorithm. In [6, p. 375] a two dimensional approach is used. In this work a three dimensional ansatz is used. The first step is the searching of boundary particles of the pile. Then straight lines are positioned with the minimization of the distance of the line to the boundary particles. The angle of repose is achieved with the average of all the angles corresponding to these lines.
In [16, 13] the oedometer experiment is performed with non-spherical particles. The influence of the particle size for spherical particles is investigated in [10]. One result of the latter work is that particle assemblies with a good graduation have a denser packing density and are less compressible [10, p. 52]. A common way for the oedometer-test is that the plate for the compression is velocity-driven. In [16, p. 422] the velocity is controlled to reduce the difference between the measured and the simulated forces.
In this work a force-driven plate was implemented. With this plate a static case is simulated for four load-steps. The implemented force-plate prevents incorrect simulation conditions where the resultant force of the particles is huger than the actual load-step.

2 DEM

Each particle is identified by the index $I \in \mathbb{M}_\mathrm{P}$ where $\mathbb{M}_\mathrm{P}$ is the set of all particle-identifiers. Each particle has a mass $\underset{I}{m}$ and a radius $\underset{I}{R}$. The location of the center of mass is denoted by $\underset{I}{\boldsymbol{S}}(t)$ and the rotational velocity by $\underset{I}{\dot{\boldsymbol{\theta}}}(t)$. The units which are used in this work are listed in table 1.

Quantity	Used units	SI-units
Mass	mg	10^{-6}kg
Length	mm	10^{-3}m
Time	ms	10^{-3}s

Table 1: Summary of the used units

In the following paragraphs the contact-displacement law is shown. Let $\mathbb{T}_\mathrm{C} = [t_\mathrm{s}, t_\mathrm{e}]$ be a time interval in which the two particles are in contact. Shortly before t_s and after t_e the two particles are not in contact.
The material parameters for all particle are identical. Hence a tupel

$$P = (E, \nu, \mu_\mathrm{PP}, \mu_\mathrm{PW}, e_\mathrm{r}, \mu_\mathrm{R,PP}, \mu_\mathrm{R,PW}) \tag{1}$$

is introduced, where the components are the Young's modulus E, Poisson ratio ν, the coefficient of friction between two particles μ_PP, the coefficient of friction between a particle and a wall μ_PW, the coefficient of restitution e_r, the coefficient of rolling resistance between two particles $\mu_\mathrm{R,PP}$ and between a particle and a wall $\mu_\mathrm{R,PW}$, respectively. In order to determine the force-displacment law for contact between particle I and J the equivalent radii, mass and Young's-

and shear modulus (cf. [9, p. 233-235]) must be determined with[1]

$$\underset{IJ}{R} := \frac{\underset{I}{R}\,\underset{J}{R}}{\underset{I}{R}+\underset{J}{R}} \quad , \quad \underset{IJ}{m} := \frac{\underset{I}{m}\,\underset{J}{m}}{\underset{I}{m}+\underset{J}{m}} \quad , \quad \overset{*}{E}(P) := \frac{E}{2\,(1-\nu^2)} \quad \text{and} \quad \overset{*}{G}(P) := \frac{G}{2\,(2-\nu)} \quad , \tag{2}$$

respectively [18, p. 242]. A nonlinear spring-dashpot model is used for the contact-displacement law [4, p. 985]. The stiffness and the viscous-damping in the normal direction is determined (cf. [9, p. 234]) with

$$\underset{IJ_\mathrm{N}}{K}(P) := \frac{4}{3}\overset{*}{E}(P)\sqrt{\underset{IJ}{R}} \qquad \text{and} \qquad \underset{IJ_\mathrm{N}}{\gamma}(t,\underset{IJ_\mathrm{N}}{\delta},P) := \beta(P)\sqrt{\underset{IJ}{m}\,\underset{IJ_\mathrm{N}}{K}(P)}\,\sqrt[4]{\underset{IJ_\mathrm{N}}{\delta}(t)} \quad , \tag{3}$$

$$\text{with} \qquad \beta(P) := \ln(e_\mathrm{r})\sqrt{\frac{5}{\ln^2(e_\mathrm{r})+\pi^2}} \quad , \tag{4}$$

where e_r is the coefficient of restitution and $\underset{IJ_\mathrm{N}}{\delta}(t)$ the overlap of the particles in the normal direction. The contact-force in the normal direction equals (cf. [18, p. 242])

$$\underset{IJ_\mathrm{N}}{F}(t,\underset{IJ_\mathrm{N}}{\delta},\underset{IJ_\mathrm{N}}{\dot{\delta}},P) := -\underset{IJ_\mathrm{N}}{K}(P)\,\underset{IJ_\mathrm{N}}{\delta}(t)^{\frac{3}{2}} - \underset{IJ_\mathrm{N}}{\gamma}(t,\underset{IJ_\mathrm{N}}{\delta},P)\,\underset{IJ_\mathrm{N}}{\dot{\delta}}(t) \quad . \tag{5}$$

The stiffness and the viscous-damping in the tangential direction (cf. [9, p. 234]) equals

$$\underset{IJ_\mathrm{T}}{K}(P) := 8\overset{*}{G}\sqrt{\underset{IJ}{R}} \qquad \text{and} \qquad \underset{IJ_\mathrm{T}}{\gamma}(t,\underset{IJ_\mathrm{T}}{\delta},P) := 2\beta(P)\sqrt{\frac{1}{6}\,\underset{IJ_\mathrm{T}}{K}(P)}\,\sqrt[4]{\underset{IJ_\mathrm{T}}{\delta}(t)} \quad , \tag{6}$$

respectively and the corresponding force could be determined with

$$\underset{IJ_\mathrm{T}}{F}(t,\underset{IJ_\mathrm{T}}{\delta},\underset{IJ_\mathrm{T}}{\dot{\delta}},\underset{IJ_\mathrm{N}}{F},P) := \min\left(\left(\left|\,\underset{IJ_\mathrm{T}}{K}(P)\,\underset{IJ_\mathrm{T}}{\delta}(t)+\underset{IJ_\mathrm{T}}{\gamma}(t,\underset{IJ_\mathrm{T}}{\delta},P)\,\underset{IJ_\mathrm{T}}{\dot{\delta}}(t)\,\right|\right),\left|\,\mu_\mathrm{PP}\,\underset{IJ_\mathrm{N}}{F}(t,\underset{IJ_\mathrm{N}}{\delta},\underset{IJ_\mathrm{N}}{\dot{\delta}},P)\,\right|\right) \quad , \tag{7}$$

where μ_PP is the coefficient of the Coloumb friction and $\underset{IJ_\mathrm{T}}{\delta}(t)$ is the tangential overlap (see [22, p. 155]).

2.1 Rolling friction

Rolling friction is introduced to decrease the translational and rotational velocity of a particle. In reality the particle velocity decreases during the movement. In order to achieve this behavior in the simulation rolling resistance is introduced (cf. [21, p. 540]). The used rolling friction model is Method-B from [21, p. 539]

$$\underset{I_\mathrm{R}}{\boldsymbol{M}}(t,P,\underset{IJ_\mathrm{N}}{F}) := -\mu_\mathrm{R,PP}\left\|\underset{IJ}{\dot{\boldsymbol{\theta}}}(t)\right\|\underset{IJ_\mathrm{N}}{F}(t,\underset{IJ_\mathrm{N}}{\delta},\underset{IJ_\mathrm{N}}{\dot{\delta}},P)\frac{\underset{I}{\dot{\boldsymbol{\theta}}}(t)}{\left\|\underset{I}{\dot{\boldsymbol{\theta}}}(t)\right\|} \quad , \tag{8}$$

where $\underset{IJ}{\dot{\boldsymbol{\theta}}}(t)$ is the relative angular velocity at the contact point.

[1] Usually the equivalent Young's modulus and the shear modulus are determined with specific values of Poisson Ratio and Young modulus.

3 COMPUTATIONAL MODEL FOR THE PILE

In this section the computational model of the dynamic simulation of the pile is described. Different ways for generating piles can be found in [2]. The simulation in this work is treated similar to the dynamic investigation of a hopper. In order to investigate only the influence of the material parameters with regard to the angle of repose the model must only depends on the material parameters. Hence the initial position of each particle must be identical for each simulation.
The sensitivity analysis is performed for two different particle sets in order to compare the sensitivity of two different particle size distributions. The particle radii for both assemblies are created by means of a normal distribution. In table 2 the interval for the restriction of the particle radii $\underset{I}{R} \in [r_\mathrm{L}; r_\mathrm{U}]$, the mean values, the standard deviation and the number of particles of the two assemblies are shown.

Particle-set	Interval for radii	Mean value	Standard deviation	Number of particles
1	$[1;3.5]$mm	2mm	0.5mm	6000
2	$[0.8;2.5]$mm	1.5mm	0.35mm	8000

Table 2: Summary of parameters for the particle generation

3.1 Particle positioning

The particle assembly consists of discs with a radius of $r_\mathrm{fu} = 20$mm in which particles are positioned like it is depicted in Fig. 2a. One of such discs is depicted in Fig. 1a.
The generation of these disc is performed with an algorithm which fills sequential annuli (see. Fig. 1a). The vertical position of the discs starts with $h = r_\mathrm{U}$. For the following discs the vertical position is increased by $2\,r_\mathrm{U}$ until the maximal height of h_fu is reached (see Fig. 2a). Then all following in sequence generated discs get the height h_fu.

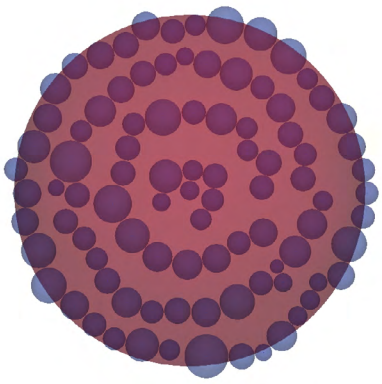

(a) Illustration of a disk of spheres for the pile investigation

(b) Measurement of the angle of repose

Figure 1: Particle-positioning for the pile assemblies

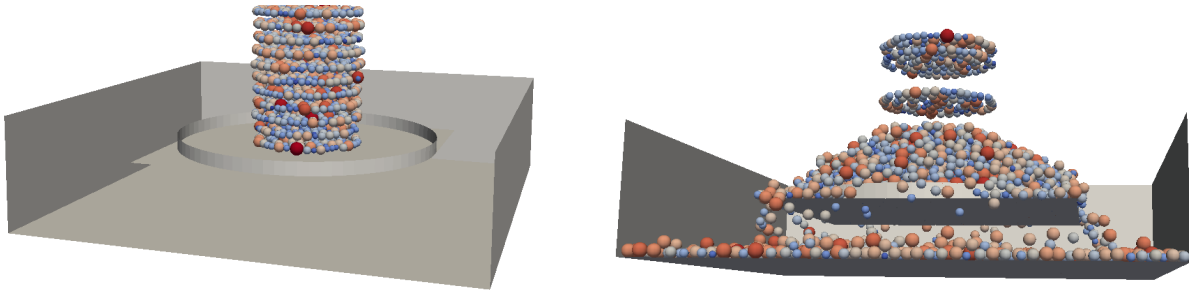

(a) Initial stage of the simulation (b) Simulation of the pile

Figure 2: Simulation of the pile

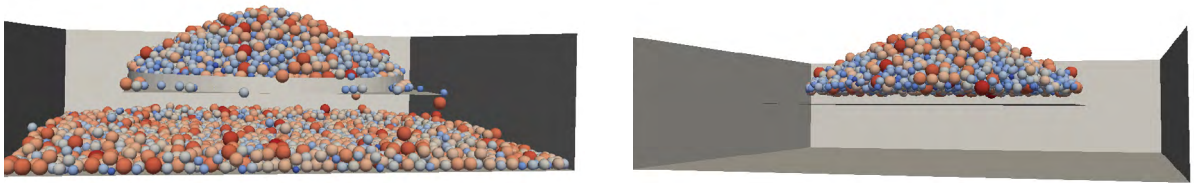

(a) Simulated pile after the ralaxation (b) Heap after the filter process

Figure 3: Finished simulation of the pile

3.2 Simulation

In order to lower the influence of the interaction between the particles and the plane a cylinder is introduced (cf. [2, p. 318]). It has a radius of $r_{\mathrm{cy}} = 50\mathrm{mm}$ and height of $h_{\mathrm{cy}} = 5\mathrm{mm}$. In the initial stage of the simulation all particles of the discs with a height below $h_{\mathrm{fu}} = 100\mathrm{mm}$ are treated, like it is depicted in Fig. 2a. In the following steps the simulation is performed for $t = \sqrt{\frac{4\,r_{\mathrm{U}}}{\|\boldsymbol{g}\|}}$, thus the upper discs covers a distance of $2\,r_{\mathrm{U}}$. Then the treated particles are appended by the next disk with a height of h_{fu} (see Fig. 2b). These steps are repeated until all particles are treated.
In order that the last inserted particles find a stable position at the end a simulation is carried out for $t = 600\mathrm{ms}$. The state after this integration is shown in Fig. 3a. Then a filter process is performed. All particles in the box or below the upper edge of the cylinder are removed, like it is depicted in Fig. 3b. During the filter-process the height of the pile h_{P} is determined.

3.3 Determination of the steepest angle of repose

A picture, in which the the steepest angle of repose of a real sandpile is measured, is shown in Fig. 1b. It can be seen that the top of the pile is rounded while the boundary of the remaining part is formed like a truncated cone. In order to determine the steepest angle of repose a cylindrical coordinate system is introduced. The origin of the coordinate system is placed at the bottom in the middle of the rounded base area of the pile. The angle of the polar axis is divided into

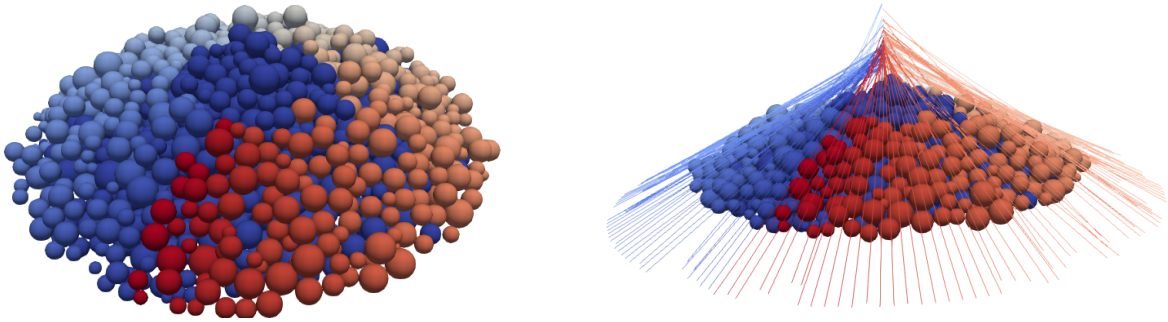

(a) Boundary particles

(b) Visualization of the truncated cone

Figure 4: Approximation of the angle of repose

$\phi_N = 180$ parts. These direction vectors are given with

$$\boldsymbol{e}_{i_\phi} := \begin{pmatrix} \cos(\phi_{i_\phi}) \\ -\sin(\phi_{i_\phi}) \end{pmatrix} \qquad \text{with} \qquad \phi_{i_\phi} := \frac{360}{\phi_N} i_\phi \qquad , \tag{9}$$

where $i_\phi = 0, \ldots, i_{\phi_N} - 1$ holds. In each direction several equidistant level of heights between $0.2h_P$ and $0.75h_P$ are defined in which the particle with the largest radial distance is searched. In Fig. 4a the particles which lie on the boundary are marked with the color which changes from red to blue with increasing i_ϕ. The dark blue particles are particles which doesn't lie on the boundary.
A line for each $\boldsymbol{e}_{i_\phi}$ is fitted with the minimization of the orthogonal distance between the particles and the line. The average angle ϕ of all these lines is the approximated angle of repose[2]. In Fig. 4b the line elements on the marked particles are shown.
The values of the measured angle of repose (see Fig. 1b) are 32° and 35°. The goodness of the fit $E_\phi(P) = (\hat{\phi} - \phi(P))^2$ is determined with the average $\hat{\phi} = 33.5°$.

4 OEDOMETER

The oedometer test is a one-dimensional compression test [19, p. 115 ff.]. A soil sample is put inside a box. On top of the soil sample a load-plate is installed on which different loads are applied. The used box has a base area of 10 cm × 10 cm and a height of 10 cm. This box prevents horizontal deformation of the soil sample. The average of six oedometer experiments is shown in Fig. 5. The settlement s is determined with $h_0 - h$ where h is the actual height of the plate and h_0 the height of the plate at the initial load step of 100 N.
The computational model consists of a rigid box which is filled with particles. In Fig. 6a the particle assembly in the box is shown after a compression with 100 N. Two assemblies are investigated. Assembly one consists of 4642 particles and has a void ratio of $e_1 = \frac{V_S}{V_P} = 0.66$, while assembly two consists of 3361 particles and has a void ratio of $e_2 = 0.67$. The quantity V_S is the solid volume taken by the particles and $V_P = 10 \cdot 10 \cdot 5\text{cm}^3 - V_S$ the volume of the voids.

[2]The implementation was performed in the bachelor thesis "Entwicklung eines Algorithmus zur Approximation des Schüttwinkels und Sensitivitätsanalyse" of Mr. B.Sc. Fabian Pfaff.

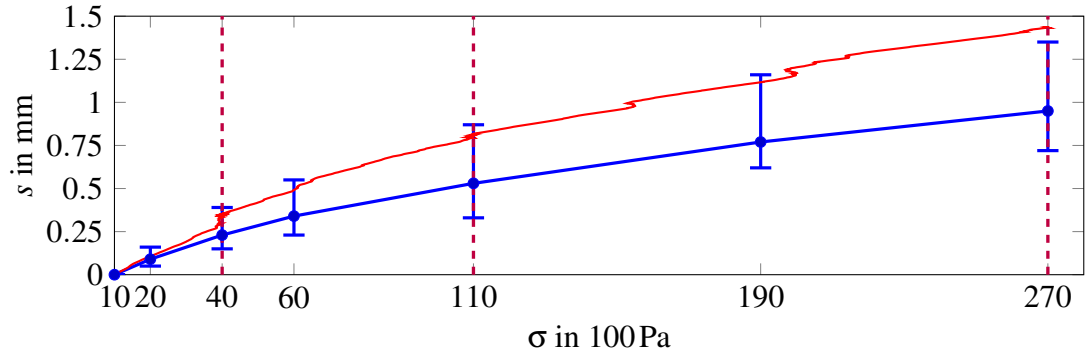

Figure 5: Stress-displacement curve for P_{120}

The force driven plate is applied for four loads L_n with $n \in \{0,1,2,3\}$. The plate iteration starts with the following three steps: The generation of a backup of the particle positions and velocities, the movement of the load-plate downwards by a trial step δ_{Ta} and an integration of $n_{\mathrm{s}} = 15000$ integration-steps.

This procedure is repeated until the resulting particle force of the force plate F_{R} satisfies the condition $F_{\mathrm{R}} > L_n$. If this condition is fulfilled an integration of $n_{\mathrm{L}} = 80000$ integration-steps is performed in order to relieve the particle force. If the resulting force F_{R} falls below L_n, the procedure with the short integrations and the backups is performed again. If the resulting force F_{R} after a long integration of n_{L} integration steps exceeds L_n, the backup of the last valid trial-step is loaded and the corresponding height of the force plate is applied. If this case occurs the trial step δ_{Ta} is reduced in each following trial-step with $\delta_{\mathrm{Ta}} \leftarrow \delta_{\mathrm{Ta}} m_{\mathrm{T}}$, where $m_{\mathrm{T}} = 0.95$ is a reduction factor. The reduction of the trial step considers the amount of the residuum $R = |F_{\mathrm{R}} - L_n|$, so that m_{T} is adjusted to the residuum. It is also considered that the trial step does not fall below a critical value of $0.05\delta_{\mathrm{T0}}$. The trial step is initialized with $\delta_{\mathrm{Ta}} \leftarrow \delta_{\mathrm{T0}} = 0.0075$. If the absolute value of the residuum is lower than the precision $R_{\mathrm{pr}} = 30$ which equals 0.03 N the iteration is finished.

With this procedure static states for the loading steps are simulated. Incorrect simulation conditions where the resulting force exceeds the plate force do not occur, since in such situations the backup of the last valid simulation state is loaded.

The simulation is performed with four loading steps $L_0 = 100\,\mathrm{N}$, $L_1 = 400\,\mathrm{N}$, $L_2 = 1100\,\mathrm{N}$ and $L_3 = 2700\,\mathrm{N}$. In Fig. 6b the iteration for the load-step L_0 is shown. The achieved precision for this load step is $(100000 - 100017.59)10^{-3}\mathrm{N} \approx 0.017\,\mathrm{N}$. The corresponding settlement $s_0 = 2.433\,795\,2\,\mathrm{mm}$ is used as a reference value for settlements of the following load-steps (see Fig. 5). The experimental settlement for the initial load-step was much smaller. The reason for this could be that the packing density must be much higher. This could be achieved with lower particle radii or/and a good graduation [10, p. 52]. In Fig. 5 the displacement-stress curve of the load-steps $L_1 = 400\mathrm{N}$, $L_2 = 1100\mathrm{N}$ and $L_3 = 2700\mathrm{N}$ is shown. In Fig. 5 and 6b the purple dashed lines marks the simulated load-steps L_i, the blue curve is the average of the measurements while the red one is the simulated curve. The error-bar in Fig. 5 represents the lowest and the highest measured values of the settlement. The quality of the simulation is quantified with the error

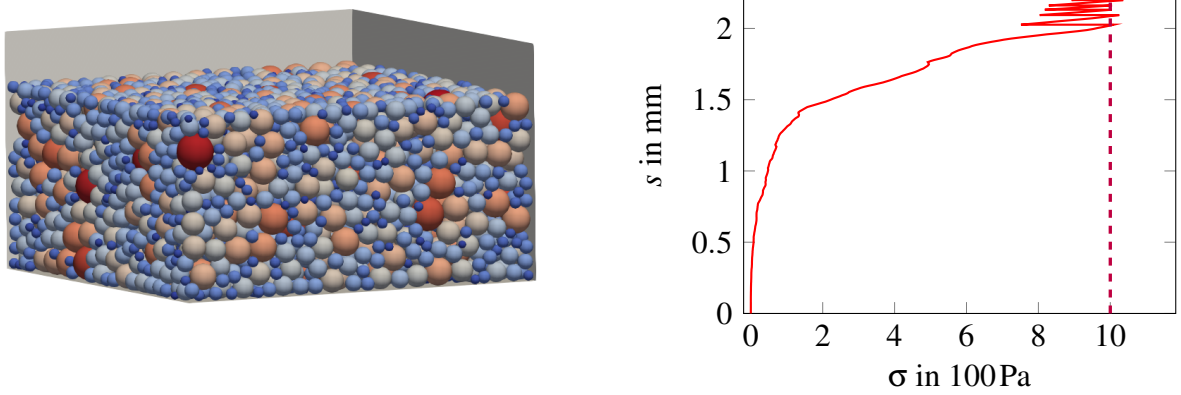

(a) Particle assembly after a compression with 100N

(b) Iteration of the load-plate with 100N for P_{120}

Figure 6: Oedometer test sample 120

measure $E_0 := \sqrt{\sum_{i=1}^{3}(\widetilde{s_i} - s_i)^2}$. which treats only the deviation of the settlements, since the deviation of the forces are negligible small due to the precision $R_{\text{pr}} = 0.03\text{N}$.

5 DESIGN OF EXPERIMENTS AND METAMODELS

Since the numerical models for the investigation of the pile and the oedometer test are time expensive the sensitivity analysis should be performed using metamodels. The numerical model of the pile described in section 3 assigns each DEM-input parameters P (see (1)) a corresponding approximation of the angle of repose $\phi(P)$. The numerical model for the oedometer-test described in section 4 is investigated with respect to the failure measure E_0. Hence both models assign each parameter tuple with a scalar for the quality of the fit with the experimental measurement.

The DOE is performed with the Latin-Hypercube-sampling (LHS) (cf. [8, p. 240]) with 160 points for the pile and 200 for the oedometer test. In Tab. 3 the investigated interval[3] for each element of P (see (1)) is shown.

On this basis four different meta-models are generated. A quadratic and a cubic polynomial response surface method (cf. [1, p. 2123]) is used. The quality of the metamodel could be determined with the regression coefficient $R^2 = \dfrac{\text{SSE}}{\text{SST}}$ where SSE is the sum of square error and SST the total square error [1, p. 2123]. In [1, p. 2123] it is mentioned that generally with increasing R^2 the quality of the fit is rising. The quadratic polynomials have a poor quality of fit for the pile- and the oedometer model in comparison to the cubic ones. An interpolating metamodel is generated as well with radial basis functions (RBF). A cubic (triharmonic) ansatz function[4] $\psi_{\text{T}}(r) = r^3$ [20, p. 55] and the thin-plate ansatz $\psi_{\text{P}}(r) = r^2 \log(r^2)$ is used [1, p. 2124].

[3]The inverval for $\mu_{\text{R,PP}}$ and $\mu_{\text{R,PW}}$ for the oedometer experiment is $[5 \cdot 10^{-5}, 0.01]$.

[4]The parameter c which is used in [1, p. 2124] is equal to one in this work.

Quantity	Interval
Young's modulus E	$E \in [10^5, 10^6]$
Poisson's ratio ν	$\nu \in [0.2, 0.4]$
Coefficient of friction between particles μ_{PP}	$\mu_{\mathrm{PP}} \in [0.7, 1.9]$
Coefficient of friction between particles and the wall μ_{PW}	$\mu_{\mathrm{PW}} \in [0.4, 1.9]$
Coefficient of restitution e_{R}	$e_{\mathrm{R}} \in [0.2, 0.6]$
Coefficient of rolling resistance between particles μ_{RPP}	$\mu_{\mathrm{RPP}} \in [0.45, 4.5]$
Coefficient of rolling resistance between particles and the wall μ_{RPW}	$\mu_{\mathrm{RPP}} \in [0.8, 5]$

Table 3: The DOE interval for the sensitivity analysis

6 Sobol' indices for the angle of repose

The global sensitivity-analysis is used to determine the influence of input variables or their combinations on the output of a system [14, p. 271]. Sobol' indices are often used since they are appropriate for the most models [17, p. 964]. A disadvantage is, that $2^n = 128$ terms [12, p. 259] must be determined for $n = 7$ input parameters. In this work the first and second order Sobol' indices are calculated for the pile and the oedometer experiments. Since the high computational effort of the numerical models the Sobol' indices are determined with the metamodels. In order to determine the Sobol' indices the input space must be defined in a n-dimensional unit cube [3, p. 3]. Hence the 7-dimensional input space (see tab. 3) for the parameter-tuple P must be transformed in a 7-dimensional unit cube $\widehat{\mathcal{P}} = [0,1]^7$. The investigated models are the quadratic and the cubic polynomial RSM, the thin-plate - and the cubic RBF of the pile experiment as well as the oedometer experiment. Each investigated model $f(\hat{P})$ with $\hat{P} \in [0,1]^7$ is decomposed in 2^n summands of different dimensions based on the Fourier-Haar series [15, p. 408] hence

$$f(\widehat{P}_1, \cdots, \widehat{P}_n) = f_0 + \sum_{i=1}^{n} f_i(\widehat{P}_i) + \sum_{i=1}^{n-1} \sum_{j=i+1}^{n} f_{ij}(\widehat{P}_i, \widehat{P}_j) + \cdots + f_{1,\ldots,n}(\widehat{P}_1, \cdots, \widehat{P}_n) \tag{10}$$

holds with $\widehat{P} = (\widehat{P}_1, \cdots, \widehat{P}_n)$. If $\widehat{P}$ is a uniform distributed random variable in $[0,1]^n$, then $f(\widehat{P})$ and the summands $f_{i_1,\ldots,i_s}(\widehat{P}_{i_1}, \cdots, \widehat{P}_{i_s})$ are random variables, too. The corresponding variances are D and $D_{i_1 \cdots i_s} = \int\limits_{\left(\hat{P}_{i_1}, \cdots, \hat{P}_{i_s}\right) \in [0,1]^s} f_{i_1,\ldots,i_s}(\hat{P}_{i_1}, \cdots, \hat{P}_{i_s})^2 \mathrm{d}\left(\hat{P}_{i_1}, \cdots, \hat{P}_{i_s}\right)$, respectively [14, p. 272].
In order to determine the variance eq. (10) could be rewritten with

$$D = \int\limits_{\hat{P}_{\mathrm{S}} \in [0,1]^n} f(\hat{P}_{\mathrm{S}})^2 \mathrm{d}\hat{P}_{\mathrm{S}} - {f_0}^2 = \sum_{i=1}^{n} \int\limits_{\hat{P}_i \in [0,1]} f_i(\hat{P}_i)^2 \mathrm{d}\hat{P}_i + \sum_{i=1}^{n} \sum_{j=1}^{n} \int\limits_{\left(\hat{P}_i, \hat{P}_j\right) \in [0,1]^2} f_{ij}(\hat{P}_i, \hat{P}_j)^2 \mathrm{d}\left(\hat{P}_i, \hat{P}_j\right) + \cdots \tag{11}$$

The Sobol' indices are determined [14, p. 272] with $S_{i_1,\ldots,i_s} := \dfrac{D_{i_1,\ldots,i_s}}{D}$. The second order Sobol' indices are lower than 0.05. Hence, they are negligible small. In Tab. 4 and 5 the first order

metamodel	E	ν	μ_{PP}	μ_{PW}	e_r	$\mu_{R,PP}$	$\mu_{R,PW}$	Res
RSM quad.	0.0166	0.0087	0.0370	0.0102	$3.7E-5$	0.8961	0.0040	0.035
RSM cub.	0.030	$9.4E-4$	0.0165	0.0132	$7.8E-6$	0.5302	0.0066	0.4483
RBF th. pl.	0.0419	0.0260	0.0091	0.0160	0.008	0.701	0.0215	0.1938
RBF cub.	0.0429	0.0275	0.0163	0.0185	0.019	0.547	0.0299	0.3302

Table 4: First order Sobol'indices for the pile experiment with assembly one

metamodel	E	ν	μ_{PP}	μ_{PW}	e_r	$\mu_{R,PP}$	$\mu_{R,PW}$	Res
RSM quad.	0.0072	0.022	0.003	0.0297	$2.3E-5$	0.9118	$7.5E-4$	0.0405
RSM cub.	0.014	0.054	0.0241	$5.5E-4$	$1.3E-6$	0.5065	0.0208	0.4096
RBF th. pl.	0.013	0.0218	0.0048	0.0015	0.020	0.759	0.010	0.2463
RBF cub.	0.016	0.019	0.0069	0.010	0.0194	0.6642	0.0207	0.3489

Table 5: First order Sobol'indices for the pile experiment with assembly two

Sobol' indices for the pile experiment are shown. The Sobol' indice for the parameter $\mu_{R,PP}$ has by far the biggest influence for all metamodels and both particle assemblies. In Tab. 6 and 7 the first order Sobol' indices for the oedometer experiment are shown. The most significant parameter of the oedometer model is by far the Young's modulus E. The sum of all indices should not exceed one. This isn't achieved in Tab. 7 for the quadratic polynomial RSM and the cubic RBF due to numerical errors.

7 CONCLUSION

In this work a sensitivity analysis with Sobol' indices is performed for the pile- and the oedometer experiment. Since the computational models of the two treated experiments are very time consuming sampling-points are generated with the Latin Hypercube sampling. On this basis four different metamodels are used to determine the first- and second order Sobol' indices. The second order Sobol' indices are negligible. The influence of the rolling friction parameter between particles is by far the most significant parameter in the pile experiment. For the oedometer experiment the Young's Modulus is by far the most significant parameter. With this information a more appropriate parameter fitting could be performed with an optimization of these parameters. A three dimensional ansatz was described to determine the angle of

metamodel	E	ν	μ_{PP}	μ_{PW}	e_r	$\mu_{R,PP}$	$\mu_{R,PW}$	Res
RSM quad.	0.9877	0.0058	0.0060	0.0018	$7.1E-6$	0.0011	0.0077	0.0103
RSM cub.	0.981	0.0017	0.0050	0.0057	$1.6E-5$	0.0059	0.0085	0.0416
RBF th. pl.	0.892	0.0011	0.0042	0.0029	0.0214	0.0026	0.0031	0.0885
RBF cub.	0.879	0.0029	0.0040	0.0049	0.0193	0.0012	0.0019	0.1066

Table 6: First order Sobol'indices for the oedometer experiment with assembly one

metamodel	E	ν	μ_{PP}	μ_{PW}	e_r	$\mu_{R,PP}$	$\mu_{R,PW}$	Res
RSM quad.	1.00	0.0094	0.0070	0.0017	$1.2E-5$	$1.8E-4$	0.0038	0.0250
RSM cub.	0.9314	0.0018	0.0067	0.0048	$2.4E-6$	0.0029	0.0069	0.0587
RBF th. pl.	0.9373	$3.4E-4$	0.0036	0.0084	0.0082	0.0021	$4.0E-4$	0.0444
RBF cub.	1.00	0.0093	0.0070	0.0017	$1.2E-5$	1.894	0.0038	0.025

Table 7: First order Sobol'indices for the pile experiment with assembly two

repose as well as a force-driven plate, which prevents incorrect simulation conditions where the resulting particle force exceeds the load-step.

REFERENCES

[1] Fang, H. and Rais-Rohani, M. and Liu, Z. and Horstemeyer, M.F. A comparative study of metamodeling methods for multiobjective crashworthiness optimization. *Computers & Structures* (2005) **83**:2122–2136.

[2] Grima, A. P. and Wypych, P. W. Discrete element simulations of granular pile formation: Method for calibrating discrete element models. *Engineering Computations* (2011)**28**:314–339.

[3] Homma, T. and Saltelli, A. Importance measures in global sensitivity analysis of nonlinear models *Reliability Engineering & System Safety* (1996) **52**:1–17.

[4] Hu, G. and Hu, Z. and Jian, B. and Liu, L. and Wan, H. On the determination of the damping coefficient of non-linear spring-dashpot system to model Hertz contact for simulation by Discrete element method *JOURNAL OF COMPUTERS* (2011) **6**:984–988.

[5] Langston, P. A. and Tüzün, U. and Heyes, D. M. Discrete element simulation of granular flow in 2D and 3D hoppers: dependence of discharge rate and wall stress on particle interactions. *Chemical Engineering Science* (1995) **50**:967–987.

[6] Lee, J. and Herrmann, H. J. Angle of repose and angle of marginal stability: Molecular dynamics of granular particles. *Journal of Physics A: Mathematical and General* (1993) **26**:373–383.

[7] Li, H. *Analysis of Off-Road Tire-Soil Interaction through Analytical and Finite Element Methods*. PhD dissertation Technischen Universität Kaiserslautern (2013).

[8] McKay, M. D. and Beckman, R. J. and Conover, W. J. Comparison of three methods for selecting values of input variables in the analysis of output from a computer code. *Technometrics* (1979) **21**:239–245.

[9] Michael, M. and Vogel, F. and Peters, B. DEM–FEM coupling simulations of the interactions between a tire tread and granular terrain. *Computer Methods in Applied Mechanics and Engineering* (2015) **289**:227–248.

[10] Minh, N. H. and Cheng, Y. P. A DEM investigation of the effect of particle-size distribution on one-dimensional compression. *Géotechnique* (2013) **63**:44-53.

[11] Rackl, M. and Hanley, K. J. A methodical calibration procedure for discrete element models. *Powder technology* (2017) **307**:73–83.

[12] Saltelli, A. and Annoni, P. and Azzini, I. and Campolongo, F. and Ratto, M. and Tarantola, S. Variance based sensitivity analysis of model output. Design and estimator for the total sensitivity index. *Computer Physics Communications* (2010) **181**:259–270.

[13] Skuodis, Š. *Modeling and Simulation in Engineering Sciences*. IntechOpen, (2016) 245–264.

[14] Sobol, I. M. Global sensitivity indices for nonlinear mathematical models and their Monte Carlo estimates. *Mathematics and computers in simulation* (2001) **55**:271–280.

[15] Sobol, I. M. Sensitivity estimates for nonlinear mathematical models. *Mathematical modelling and computational experiments* (1993) **1**:407–414.

[16] Stahl, M. and Konietzky, H. Discrete element simulation of ballast and gravel under special consideration of grain-shape, grain-size and relative density. *Granular Matter* (2011) **13**:417–428.

[17] Sudret, B. Global sensitivity analysis using polynomial chaos expansions. *Reliability engineering & system safety* (2008) **93**:964–979.

[18] Tsuji, Y. and Tanaka, T. and Ishida, T. Lagrangian numerical simulation of plug flow of cohesionless particles in a horizontal pipe *Powder technology* (1992) **71**:239–250.

[19] Verruijt, A. *An Introduction to Soil Mechanics*. Springer Switzerland Vol. 30, (2017).

[20] Yaghouti, M. and Azarboni, H. R. Determining optimal value of the shape parameter c in RBF for unequal distances topographical points by Cross-Validation algorithm. *Journal of Mathematical Modeling* (2017) **5**:53–60.

[21] Zhou, Y. C. and Wright, B. D. and Yang, R. Y. and Xu, B. H. and Yu, A. B. Rolling friction in the dynamic simulation of sandpile formation *Physica A: Statistical Mechanics and its Applications* (1999) **269**:536–553.

[22] Haff, P. K. *Granular Matter: an interdisciplinary approach* Springer New-York (1994)

[23] Jahn, M. and Meywerk, M. On the transformation laws for the macro to micro transformation *PAMM* (2019) accepted for puclication.